

Towards a Pixel TPC: construction and test of a 32 chip GridPix detector

M. van Beuzekom^a, Y. Bilevych^b, K. Desch^b, S. van Doesburg^a,
H. van der Graaf^a, J. Kaminski^b, P.M. Kluit^a, N. van der Kolk^a, C.
Ligtenberg^a, G. Raven^a, J. Timmermans^a

^a*Nikhef, Science Park 105, 1098 XG Amsterdam, The Netherlands*

^b*Physikalisches Institut, University of Bonn, Nussallee 12, 53115 Bonn,
Germany*

Abstract

A Time Projection Chamber module with 32 GridPix chips was constructed and the performance was measured using data taken in a test beam at DESY in 2012. The GridPix chips each consist of a Timepix3 chip with integrated amplification grid and have a high efficiency to detect single ionisation electrons. In the test beam setup, the module was placed in between two sets of Mimosas silicon detector planes that provided external high precision tracking and the whole detector setup was slid into the PCMag magnet at DESY. The analysed data were taken at electron beam energies of 5 and 6 GeV and at magnetic fields of 0 and 1 Tesla(T).

The result for the transverse diffusion coefficient D_T is $287 \mu\text{m}/\sqrt{\text{cm}}$ at $B = 0$ T and D_T is $121 \mu\text{m}/\sqrt{\text{cm}}$ at $B = 1$ T. The longitudinal diffusion coefficient D_L is measured to be $268 \mu\text{m}/\sqrt{\text{cm}}$ at $B = 0$ T and $252 \mu\text{m}/\sqrt{\text{cm}}$ at $B = 1$ T. Results for the tracking systematical uncertainties in xy were measured to be smaller than $14 \mu\text{m}$ with and without magnetic field. The tracking systematical uncertainties in z were smaller than $14 \mu\text{m}$ ($B = 0$ T) and $22 \mu\text{m}$ ($B = 1$ T). Finally, the result for the dEdx resolution for a MIP particle based on a 1 meter track and a realistic GridPix coverage of 60% was measured to be 4% in a 1 T magnetic field.

Keywords: Micromegas, gaseous pixel detector, micro-pattern gaseous

*Corresponding author. Telephone: +31 20 592 2000
Email address: s01@nikhef.nl (P.M. Kluit)
Preprint submitted to Elsevier

30 **1. Introduction**

31 Earlier publications on a single chip [1] and four chip (quad) GridPix detec-
 32 tors [2] showed the potential of the GridPix technology and the large range of
 33 applications for these devices [3]. In particular, it was demonstrated that single
 34 ionisation electrons can be detected with high efficiency and great precision, al-
 35 lowing an excellent track 3D position measurements and particle identification
 36 based on the number of electrons and clusters.

37 As a next step towards a Pixel Time Projection Chamber for a future col-
 38 lider experiment [4], [5], a module consisting of 32 GridPix chips based on the
 39 Timepix3 chip was constructed.

40 A GridPix detector consists of a CMOS pixel Timepix3 chip [6] with in-
 41 tegrated amplification grid added by MEMS postprocessing techniques. The
 42 Timepix3 chip can be operated with a low threshold of $515 e^-$, and has a low
 43 equivalent noise charge of about $70 e^-$. The GridPix single chip and quad de-
 44 tectors have a very fine granularity of $55 \mu\text{m} \times 55 \mu\text{m}$ and a high efficiency to
 45 detect single ionisation electrons.

46 Based on the experience gained with these detectors a 32 GridPix chip mod-
 47 ule - consisting of 8 quads - was built. A drift box defining the electric field
 48 and gas envelop was constructed. A readout system for up to 128 chips with 4
 49 multiplexers readout by one speedy pixel detector readout board was designed.
 50 After a series of tests using the laser setup in the laboratory at Nikhef [7], the
 51 detector was taken to DESY for a two week test beam campaign.

52 At DESY the 32 chip detector was placed in between two sets of Mimosas
 53 silicon detector planes and mounted on a movable stage. The whole detector
 54 setup was slid into the centre of the PCMag magnet at DESY. A trigger
 55 was provided by a scintillator counter. The data were taken at different stage
 56 positions and electron beam energies of 5 and 6 GeV and at magnetic fields of 0
 57 and 1 Tesla(T). The performance of the 32 GridPix chip module was measured

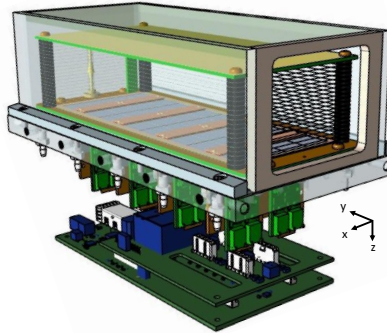


Figure 1: Schematic 3-dimensional render of the 8-quad module detector for illustration purposes.

58 using these data sets.

59 1.1. 32 GridPix chip module

60 A 32 GridPix chip module was built using the quad module [2] as a basic
 61 building block. The quad module consists of four GridPix chips and is optimised
 62 for a high fraction of sensitive area of 68.9%. The external dimensions are
 63 39.6 mm \times 28.38 mm. The four chips which are mounted on a cooled base plate
 64 (COCA), are connected with wire bonds to a common central 6 mm wide PCB.
 65 A 10 mm wide guard electrode is placed over the wire bonds 1.1 mm above the
 66 aluminium grids, in order to prevent field distortions of the electric drift field.
 67 The guard is the main inactive area, and its dimensions are set by the space
 68 required for the wire bonds. On the back side of the quad module, the PCB
 69 is connected to a low voltage regulator. The aluminium grids of the GridPixes
 70 are connected by 80 μ m insulated copper wires to a high voltage (HV) filtering
 71 board. The quad module consumes about 8 W of power of which 2 W is used in
 72 the LV regulator.

73 Eight quad modules were embedded in a box, resulting in a GridPix module
 74 with a total of 32 chips. A schematic 3-dimensional drawing of the detector is
 75 shown in Figure 1. A schematic drawing of the quads in the module is shown
 76 in Figure 2, where also the beam direction is indicated.

77 The internal dimensions of the box are 79 mm along the x -axis, 192 mm along
 78 the y -axis, and 53 mm along the z -axis (drift direction), and it has a maximum
 79 drift length (distance between cathode and readout anode) of 40 mm. The drift
 80 field is shaped by a series of parallel CuBe field wires of 50 μm diameter with a
 81 wire pitch of 2 mm and guard strips are located on all of the four sides of the
 82 active area. In addition, six guard wires - shown with dashed line in Figure 2
 83 - are suspended over the boundaries of the chips, where no guard is present, to
 84 minimize distortions of the electric drift field. The wires are located at a distance
 85 of 1.15 mm from the grid planes, and their potential is set to the potential at
 86 this drift distance. The box has two Kapton 50 μm windows to allow the beam
 87 to pass with minimal multiple scattering.

88 The data acquisition system of the quad module was adopted to allow for
 89 multiple quads to be readout. A multiplexer card was developed that handles
 90 four quads or 16 chips and combines the Timepix3 data into one data stream.
 91 For the 32 GrixPix module two multiplexers are connected to a speedy pixel
 92 detector readout (SPIDR) board [8] [9] that controls the chips and readout pro-
 93 cess. The readout speed per chip is 160 Mbps and for the multiplexer 2.56 Gbps
 94 this corresponds to a maximum rate of 21 MHits/s. For each pixel the precise
 95 Time of Arrival (ToA) using a 640 MHz TDC and the time over threshold (ToT)

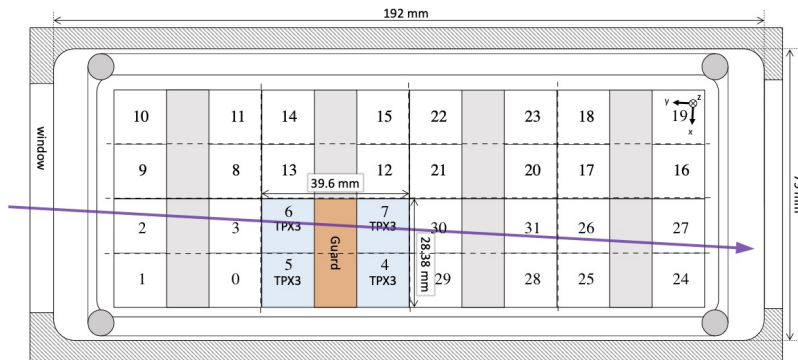


Figure 2: Schematic drawing of the 8-quad module detector with one example quad. The chips are numbered and the beam direction is shown in purple.

96 are measured.

97 The gas volume of 780 ml is continuously flushed at a rate of ~ 50 ml/min
98 with premixed T2K TPC gas. This gas is a mixture consisting of 95 % Ar, 3 %
99 CF_4 , and 2 % iC_4H_{10} suitable for large TPCs because of the relatively high drift
100 velocity and the low diffusion in a magnetic field.

101 *1.2. Experimental setup*

102 In preparation of the two weeks DESY test beam campaign, a support frame
103 was designed to move the 32 chip GridPix module in the transverse plane by a
104 remotely controlled stage thus that the whole detector volume could be probed.
105 The support frame also held three Mimosa 26 silicon detector planes [10] placed
106 in front of the detector and and three Mimosa planes behind the detector.
107 At DESY the Mimosa silicon detector planes that were provided by the test
108 beam coordinators were mounted. The whole detector setup was slid into
109 the centre of the PCMAG magnet at the DESY test beam facility II [11]. A
110 trigger was provided by a scintillator counter. The data were taken at different
111 stage positions to cover the whole sensitive TPC volume. Runs with electron
112 beam energies of 5 and 6 GeV and at magnetic fields of 0 and 1 Tesla(T) were
113 analysed.

114 A photograph of the detector setup in the PCMAG magnet is shown in
115 Figure 3.

116 The experimental and environmental parameters such as temperature, pres-
117 sure, gas flow, oxygen content were measured and logged by the windows op-
118 erated slow control system. The experimental parameters are summarised in
119 Table 1. The chips were cooled by circulating glycol through the cooling chan-
120 nels in the module carrier plate. The cooling blocks of the concentrators were
121 further cooled by blowing pressurised air on them.

122 The data was produced in four main data streams: one stream produced by
123 the Mimosa Telescope, two data streams by the two Timepix concentrators and
124 one trigger stream. A scintillator provided a trigger signal to the Trigger Logic
125 Unit (TLU) [12] that sends a signal to the trigger SPIDR and telescope readout.

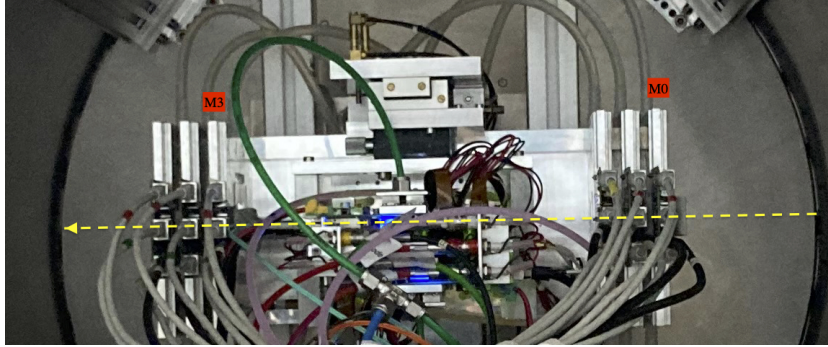


Figure 3: Photo of the detector setup at the centre of the PCMAG magnet. The Mimosa planes M0 and M3 are indicated in red as well as the beam direction (yellow). Centrally, the stager positions the TPC module thus that the beam passes through.

Table 1: Overview of the experimental parameters. The ranges indicate the variation over the data taking period

Number of analysed runs at B=0 (1) Tesla	6 (8)
Run duration	10-90 minutes
Number of triggers	3-100 k
E_{drift}	280 V/cm
V_{grid}	340 V
Threshold	550 e ⁻
Gas Temperature	303.3-306.6 K
Pressure	1011 – 1023 mbar
Oxygen concentration	240 - 620 ppm
Water vapour concentration	2000 - 7000 ppm

126 The data acquisition system of the Telescope and trigger SPIDR injected a
127 timestamp into their respective data streams. Hits from the Mimosa planes
128 were collected with a sliding window of -115 ms to 230 ms of the trigger. The
129 data acquisition of the concentrator and the trigger SPIDR were synchronized at
130 the start of the run. By comparing the time stamps in these streams, Telescope
131 tracks and TPC tracks could be matched. Unfortunately, the SPIDR trigger
132 had - due to a cabling mistake at the output of the TLU - a common 25 nsec
133 jitter.

134 In the first week of the test beam period it was found out that three HV
135 cables had a bad connection. The cables were replaced and the module could
136 be fully operated. Unfortunately, after a short data taking period one of the
137 chips (nr 11) developed a short circuit and the HV on the grid of the chip
138 was disconnected. Only after the test beam data taking period the module was
139 repaired in the clean room in Bonn.

140 **2. Analysis**

141 *2.1. Telescope Track reconstruction procedure*

142 The data of the Telescope is decoded and analysed using the Corryvreckan
143 software package [13]. The track model used for fitting was the general broken
144 lines (GBL) software [14]. The code was extended and optimized to fit curved
145 broken lines for the data with a magnetic field. The telescope planes were iter-
146 atively aligned using the standard alignment software provided by the package.
147 The single point Mimosa resolution is $4\ \mu\text{m}$ in x and $6\ \mu\text{m}$ in z (drift direction).

148 Telescope tracks were selected with at least 5 out of the 6 plane on the track
149 and a total χ^2 of better than 25 per degree of freedom. The uncertainties on the
150 Telescope track prediction in the middle of the GridPix module are dominated
151 by multiple scattering. For a 6 GeV track with no magnetic field they can be
152 measured comparing the predictions from the two telescope arms. The expected
153 uncertainty in x and z is $26\ \mu\text{m}$ on average.

154 *2.2. TPC Track reconstruction procedure*

155 GridPx hits are selected requiring a minimum time over threshold ToT of
156 0.15 μ s. The drift time is defined as the measured time of arrival minus the
157 trigger time recorded in the trigger SPIDR data stream. The drift time was
158 corrected for time slewing [2] using the measured time over threshold (ToT)
159 and the formula 1:

$$\delta t = \frac{18.6(ns)}{\text{ToT} + 0.1577(\mu s)}. \quad (1)$$

160 Furthermore, small time shifts corrections - with an odd-even and a 16×2 pixels
161 structure - coming from the TPX3 clock distribution were extracted from the
162 data and applied.

163 The z -coordinate - i.e. the drift length - was calculated from the drift time
164 and the drift velocity. GridPix hits outside a Telescope acceptance window in
165 x (± 15 mm) and z (± 7.5 mm) were not used in the track finding and recon-
166 struction. Based on a Hough transform an estimate of the TPC track position
167 and angles in the middle of the module (at $y = 1436$ pixels) was obtained. This
168 estimate was used to collect the hits around the TPC track and fit the track
169 parameters. For this fit a straight line (B=0 Tesla) or a quadratic track (B=1
170 Tesla) model was used. In the fit, the expected uncertainties per hit σ_x and
171 σ_z were used. The fit was iterated three times to perform outlier removal at
172 respectively 10, 5 and 2.5 sigma level. A TPC track was required to have a least
173 100 hits in each concentrator. At least 25% of the total number of hits should
174 be on track and the χ^2 per degree of freedom has to be less than 3 in xy and z .
175 All track parameters were expressed at a plane the middle of the TPC.

176 The drift velocity was calibrated per run comparing the Telescope tracks to
177 the TPC hits. For the B=0 field runs it varies between 0.0616 and 0.0630 mm/ns.
178 For the B=1 Tesla runs between 0.0572 and 0.0591 mm/ns. The variation comes
179 mainly from the changes in the relative humidity of the gas volume due to small
180 leaks. The individual TPX3 chips were aligned fitting a shift in x (z) and two
181 slopes $dx(z)/d \text{ row}(\text{column})$. The alignment was done per run, because the

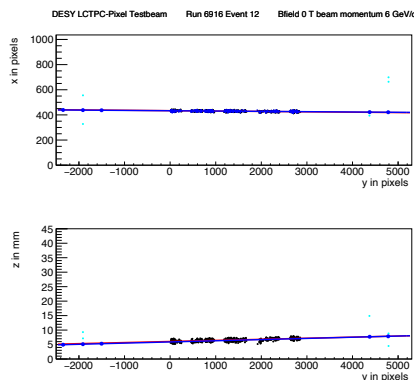


Figure 4: An event display for run 6913 without B field, with 1293 TPC hits (black dots) in the precision plane (xy) and driftplane (zy). The fitted TPC track (red line) with 1130 hits on is and the telescope track (blue line) with 5 Mimosa planes (blue hits) on track are shown. In green the off track Mimosa hits are shown.

182 detector was moved in and x and or z for each run. The fitted slopes also
 183 corrected for small shifts and rotations (3D) in the nominal chip position.

184 An example event run 6913 without B field with a TPC and a telescope
 185 track is shown in figure 4. The TPC is located between $y = 0$ and 2872 pixels.
 186 Three Mimosa planes are located at $y \lesssim -1000$ and three at $y \gtrsim 4000$ pixels.

187 2.3. Track selections

188 In order to study the single electron resolution for the data with and without
 189 magnetic field, additional selections on the Telescope and TPC tracks were
 190 applied to select high quality tracks. Due to the trigger time jitter of 25 nsec,
 191 the prediction of the telescope track in z must be used as the reference for z .
 192 Secondly, the z hits of the TPC track were fitted to correct for the common
 193 time shift and the z residuals were calculated with respect to the fitted TPC
 194 track. In the xy plane the residuals of TPC hits with respect to the telescope
 195 track were used to extract the single electron resolution in xy . For the resolution
 196 studies runs at three different z stage positions of the TPC were selected where
 197 the beam gave hits in the central chips. The data of 14 central chips (9, 12, 21,
 198 21, 20, 17, 16, 2, 3, 6, 7, 30, 21, 26 and 27) was used. Two chips (8 and 13)

Table 2: Table with track selection cuts

Event Selection
$ x_{\text{TPC}} - x_{\text{Telescope}} < 0.3 \text{ mm}$
$ z_{\text{TPC}} - z_{\text{Telescope}} < 2.0 \text{ mm}$
$ dx/dy_{\text{TPC}} - dx/dy_{\text{Telescope}} < 4 \text{ mrad}$
$ dz/dy_{\text{TPC}} - dz/dy_{\text{Telescope}} < 2 \text{ mrad}$

199 were left out because of the E field deformations caused by the short circuit in
 200 chip 11.

201 The track selections are summarized in table 2.

202 3. Results

203 3.1. Number of hits

204 The distribution of the number of TPC track hits per chip - without requiring
 205 a matched Telescope track - are shown in figure 5 for the data without magnetic
 206 field and for the B = 1 Tesla data.

207 The mean number of hits is measured to be 124 and 89 in the B=0 and 1
 208 Tesla data sets. The most probable values are respectively 87 and 64. Note that
 209 the B=0 data has a much larger Landau-like tail than the 1 Tesla data. Also
 210 the fluctuations in the core of the distribution are larger. The mean time over
 211 threshold for the B=0 T is 0.68 μs and 0.86 μs at a 1 Tesla field. This means
 212 that the deposited charge per hit is smaller for the 0 T data. The most probable
 213 value for the total deposited charge is similar for both data sets. These numbers
 214 are in agreement with the predictions of [15] 106 electron-ion pairs for an 6 GeV
 215 electron at B=0 , crossing 236 pixels or 12.98 mm and a detector running at
 216 85% single electron efficiency.

217 3.2. Hit resolution in the pixel plane

218 The resolution of the hits in the transverse plane (xy) was measured as a
 219 function of the predicted drift position (z). Only hits are used crossing the

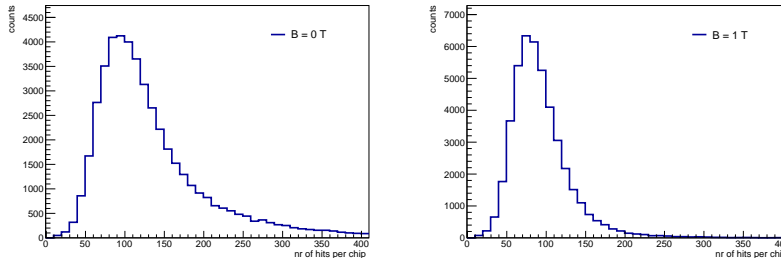


Figure 5: Distribution of the number of hits per per chip for B=0 (left) B=1 Tesla data.

220 fiducial region defined by central core of the beam and staying 20 pixels away
 221 from the chip edges. The resolution for the detection of ionisation electrons σ_x
 222 is given by:

$$\sigma_x^2 = \frac{d_{\text{pixel}}^2}{12} + d_{\text{track}}^2 + D_T^2(z - z_0), \quad (2)$$

223 where d_{pixel} is the pixel pitch size, d_{track} the uncertainty from the track predic-
 224 tion, z_0 is the position of the grid, and D_T is the transverse diffusion coefficient.
 225 The resolution at zero drift distance $d_{\text{pixel}}/\sqrt{12}$ was fixed to $15.9 \mu\text{m}$ and d_{track}
 226 to $30 \mu\text{m}$ for B=0 and $42 \mu\text{m}$ for B = 1 Tesla data.

227 The expression (2) - leaving z_0 and the D_T as free parameters - is fitted to
 228 the B=0 T data shown in Figure 6. The fit gives a transverse diffusion coefficient
 229 D_T of $287 \mu\text{m}/\sqrt{\text{cm}}$ with negligible statistical uncertainty. The measured value
 230 is in agreement with value of $287 \mu\text{m}/\sqrt{\text{cm}} \pm 4\%$ predicted by the gas simulation
 231 software Magboltz [16]. The values of the diffusion coefficients depend on the
 232 humidity that was not precisely measured during the testbeam. The humidity
 233 strongly affects the drift velocity. Therefore the drift velocity prediction from
 234 Magboltz was used to determine the water content per run and predictions for
 235 the diffusion coefficients could be obtained.

236 A fit to the B=1 T data shown in Figure 6 gives a transverse diffusion
 237 coefficient D_T of $121 \mu\text{m}/\sqrt{\text{cm}}$ with negligible statistical uncertainty. The mea-
 238 sured value is in agreement with the value of $119 \mu\text{m}/\sqrt{\text{cm}} \pm 2\%$ predicted by
 239 Magboltz.

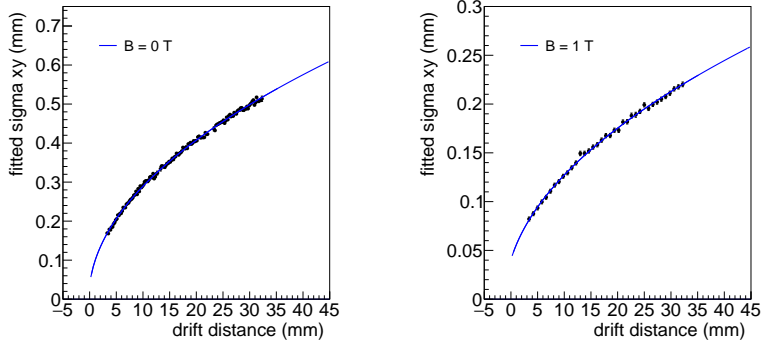


Figure 6: Measured hit resolution in the pixel plane (back points) fitted with the resolution function according to equation (2) (blue line).

240 4. Conclusion and outlook

241 A Time Projection Chamber module with 32 GridPix chips was constructed
 242 and the performance was measured using data taken in a test beam at DESY in
 243 2012. The analysed data were taken at electron beam energies of 5 and 6 GeV
 244 and at magnetic fields of 0 and 1 Tesla(T).

245 The result for the transverse diffusion coefficient D_T is $287 \mu\text{m}/\sqrt{\text{cm}}$ at $B =$
 246 0 T and D_T is $121 \mu\text{m}/\sqrt{\text{cm}}$ at $B = 1 \text{ T}$. The longitudinal diffusion coefficient
 247 D_L is measured to be $268 \mu\text{m}/\sqrt{\text{cm}}$ at $B = 0 \text{ T}$ and $252 \mu\text{m}/\sqrt{\text{cm}}$ at $B = 1 \text{ T}$.
 248 Results for the tracking systematical uncertainties in xy were measured to be
 249 smaller than $14 \mu\text{m}$ with and without magnetic field. The tracking systematical
 250 uncertainties in z were smaller than $14 \mu\text{m}$ ($B = 0 \text{ T}$) and $22 \mu\text{m}$ ($B = 1 \text{ T}$).

251 Acknowledgements

252 The 32 Gridpix module could not be constructed without the enormous effort
 253 and creative energy that Fred Hartjes has invested in it over several years. This
 254 research was funded by the Netherlands Organisation for Scientific Research
 255 NWO. The authors want to thank the support of the mechanical and electronics
 256 departments at Nikhef and the detector laboratory in Bonn. The measurements

257 leading to these results have been performed at the Test Beam Facility at DESY
258 Hamburg (Germany), a member of the Helmholtz Association (HGF).

259 **References**

- 260 [1] C. Ligtenberg, et al., Performance of a GridPix detector based on the
261 Timepix3 chip, Nucl. Instrum. Meth. A 908 (2018) 18–23. [arXiv:1808.](https://arxiv.org/abs/1808.04565)
262 [04565](https://arxiv.org/abs/1808.04565), [doi:10.1016/j.nima.2018.08.012](https://doi.org/10.1016/j.nima.2018.08.012).
- 263 [2] C. Ligtenberg, et al., Performance of the GridPix detector quad, Nucl.
264 Instrum. Meth. A 956 (2020) 163331. [arXiv:2001.01540](https://arxiv.org/abs/2001.01540), [doi:10.1016/](https://doi.org/10.1016/j.nima.2019.163331)
265 [j.nima.2019.163331](https://doi.org/10.1016/j.nima.2019.163331).
- 266 [3] J. Kaminski, Y. Bilevych, K. Desch, C. Krieger, M. Lupberger, GridPix de-
267 tectors - introduction and applications, Nucl. Instrum. Meth. A845 (2017)
268 233–235. [doi:10.1016/j.nima.2016.05.134](https://doi.org/10.1016/j.nima.2016.05.134).
- 269 [4] C. Ligtenberg, A GridPix TPC readout for the ILD experiment at the fu-
270 ture International Linear Collider, Ph.D. thesis, University of Amsterdam
271 (2021).
272 URL [https://www.nikhef.nl/pub/services/biblio/theses_pdf/](https://www.nikhef.nl/pub/services/biblio/theses_pdf/thesis_C_Ligtenberg)
273 [thesis_C_Ligtenberg](https://www.nikhef.nl/pub/services/biblio/theses_pdf/thesis_C_Ligtenberg)
- 274 [5] M. Lupberger, Y. Bilevych, H. Blank, D. Danilov, K. Desch, A. Hamann,
275 J. Kaminski, W. Ockenfels, J. Tomtschak, S. Zigann-Wack, Toward the
276 Pixel-TPC: Construction and Operation of a Large Area GridPix Detector,
277 IEEE Trans. Nucl. Sci. 64 (5) (2017) 1159–1167. [doi:10.1109/TNS.2017.](https://doi.org/10.1109/TNS.2017.2689244)
278 [2689244](https://doi.org/10.1109/TNS.2017.2689244).
- 279 [6] T. Poikela, J. Plosila, T. Westerlund, M. Campbell, M. De Gaspari,
280 X. Llopart, V. Gromov, R. Kluit, M. van Beuzekom, F. Zappone,
281 V. Zivkovic, C. Brezina, K. Desch, Y. Fu, A. Kruth, Timepix3: a 65K
282 channel hybrid pixel readout chip with simultaneous ToA/ToT and sparse
283 readout, JINST 9 (05) (2014) C05013.

- 284 [7] F. Hartjes, A diffraction limited nitrogen laser for detector calibration in
285 high energy physics, Ph.D. thesis, University of Amsterdam (1990).
286 URL [https://www.nikhef.nl/pub/services/biblio/theses_pdf/](https://www.nikhef.nl/pub/services/biblio/theses_pdf/thesis_F_Hartjes.pdf)
287 [thesis_F_Hartjes.pdf](https://www.nikhef.nl/pub/services/biblio/theses_pdf/thesis_F_Hartjes.pdf)
- 288 [8] J. Visser, M. van Beuzekom, H. Boterenbrood, B. van der Heijden, J. I.
289 Muñoz, S. Kulis, B. Munneke, F. Schreuder, SPIDR: a read-out system for
290 Medipix3 & Timepix3, *Journal of Instrumentation* 10 (12) (2015) C12028.
291 doi:10.1088/1748-0221/10/12/C12028.
- 292 [9] B. van der Heijden, J. Visser, M. van Beuzekom, H. Boterenbrood, S. Kulis,
293 B. Munneke, F. Schreuder, SPIDR, a general-purpose readout system for
294 pixel ASICs, *JINST* 12 (02) (2017) C02040. doi:10.1088/1748-0221/12/
295 02/C02040.
- 296 [10] H. Jansen, S. Spannagel, J. Behr, A. Bulgheroni, G. Claus, E. Corrin,
297 D. Cussans, J. Dreyling-Eschweiler, D. Eckstein, T. Eichhorn, M. Goffe,
298 I. M. Gregor, D. Haas, C. Muhl, H. Perrey, R. Peschke, P. Roloff, I. Ru-
299 binskiy, M. Winter, Performance of the eudet-type beam telescopes, *EPJ*
300 *Techniques and Instrumentation* 3 (1) (2016) 7. doi:10.1140/epjti/
301 s40485-016-0033-2.
- 302 [11] J. D.-E. e. a. R. Diener, The desy ii test beam facility', *Nuclear Instruments*
303 *and Methods in Physics Research. Section A: Accelerators, Spectrometers,*
304 *Detectors and Associated Equipment* 922 (2019) 265–286. arXiv:1807.
305 09328, doi:10.1016/j.nima.2018.11.133.
- 306 [12] D. Cussans, Description of the JRA1 Trigger Logic Unit (TLU), v0.2c,
307 EUDET Collaboration (2009).
308 URL [https://www.eudet.org/e26/e28/e42441/e57298/](https://www.eudet.org/e26/e28/e42441/e57298/EUDET-MEMO-2009-04.pdf)
309 [EUDET-MEMO-2009-04.pdf](https://www.eudet.org/e26/e28/e42441/e57298/EUDET-MEMO-2009-04.pdf)
- 310 [13] J. Kröger, S. Spannagel, M. Williams, User manual for the corrvrekan
311 test beam data reconstruction framework, version 1.0 (2019). arXiv:1912.
312 00856.

- 313 [14] C. Kleinwort, General broken lines as advanced track fitting method, Nu-
314 clear Instruments and Methods in Physics Research Section A: Accelerators,
315 Spectrometers, Detectors and Associated Equipment 673 (2012) 107–
316 110. doi:10.1016/j.nima.2012.01.024.
- 317 [15] R. Veenhof, Garfield - simulation of gaseous detectors, version 9, Reference
318 W5050 (1984-2010).
319 URL <https://garfield.web.cern.ch>
- 320 [16] S. F. Biagi, Monte Carlo simulation of electron drift and diffusion in count-
321 ing gases under the influence of electric and magnetic fields, Nucl. Instrum.
322 Meth. A421 (1-2) (1999) 234–240. doi:10.1016/S0168-9002(98)01233-9.